Received 11 November 2019; revised 11 January 2020 and 11 February 2020; accepted 16 February 2020. Date of publication 19 February 2020; date of current version 27 February 2020. The review of this paper was arranged by Editor S. Vaziri.

Digital Object Identifier 10.1109/JEDS.2020.2975074

Collaborative Applying the Ultra-low-k Dielectric and the High-k Dielectric Materials for Performance Enhancement in Coupled Multilayer Graphene Nanoribbon Interconnects

PENG XU AND ZHONGLIANG PAN

School of Physics and Telecommunication Engineering, South China Normal University, Guangzhou 510006, China

CORRESPONDING AUTHOR: Z. PAN (e-mail: panzhongliang@m.scnu.edu.cn)

This work was supported in part by the Guangzhou Science and Technology Project under Grant 201904010107, in part by the Guangdong Provincial Natural Science Foundation of China under Grant 2019A1515010793, in part by the Guangdong Province Science and Technology Project under Grant 2016B090918071, and in part by the National Natural Science Foundation of China under Grant 61072028.

ABSTRACT Based on transmission line modeling, a new technology of collaborative applying the ultra-low-k dielectric and the high-k dielectric materials in coupled multilayer graphene nanoribbon (MLGNR) interconnects (i.e., case 4) to reduce propagation delay and to expand 3-dB bandwidth of the conventional pristine (undoped) MLGNR interconnects is proposed in this paper. By using the decoupling technique and ABCD parameter matrix approach, the transfer function of the equivalent circuit model for coupled MLGNR interconnects is derived to obtain step response, propagation delay, transfer gain and 3-dB bandwidth under in-phase and out-of-phase crosstalk modes at global level of 7.5 nm technology node, which is based on the defined four cases. The results show that the maximum reduction of propagation delay between the proposed new technology (case 4) and the conventional MLGNR interconnects (case 1) can reach 15.911 ns at out-of-phase crosstalk mode for an interconnect length of 4000 μm. The corresponding 3-dB bandwidth for them can be expanded over 2.978 times in the same length as the former. It is demonstrated that the proposed case 4 can obviously reduce the propagation delay and enhance the transfer gain and 3-dB bandwidth compared with the conventional case 1. Moreover, it is found that the coupled MLGNR interconnect under in-phase mode outperform that under out-of-phase mode in terms of propagation delay, transfer gain and 3-dB bandwidth at the same condition. In addition, it is manifested that the victim line of two-line coupled MLGNR interconnects have lesser propagation delay, higher transfer gain and larger 3-dB bandwidth, as compared to three-line coupled MLGNR interconnects at the same case. The proposed new technology in this paper would be beneficial to improve the performance of MLGNR interconnects and to provide the guidelines for the design of next generation on-chip MLGNR interconnect system.

INDEX TERMS MLGNR interconnects, step response, propagation delay, transfer gain, 3-dB bandwidth, ultra-low-k dielectric, high-k dielectric.

I. INTRODUCTION

With the continuous advancement of semiconductor manufacturing technology in very large-scale integrated (VLSI) circuits, a series of performance degradation on the conventional copper (Cu) based interconnects have been reported, such as the larger resistivity, electro-migration and smaller

This work is licensed under a Creative Commons Attribution 4.0 License. For more information, see http://creativecommons.org/licenses/by/4.0/

current capacity problems [1]–[3]. Due to the outstanding electrical, mechanical and thermal properties, graphene material has captured considerable attention from the researchers that is regarded as a potential alternative to the traditional Cu for next-generation on-chip interconnect applications [4], [5]. High quality graphene has a long mean free path (MFP) on the order of several micrometers far over Cu material, which leads to a lower resistivity and achieves the ballistic transport at the shorter interconnects [6]–[8]. Moreover, graphene can carry a higher current density of the order of 10^9 A/cm^2 in comparison to its Cu counterpart that effectively alleviates the electro-migration phenomenon [9], [10]. Graphene nanoribbon (GNR) is a narrow strip of graphene sheet that can be divided into multilayer GNR (MLGNR) and single-layer GNR (SLGNR) according to its stacked number of layers. Owing to the larger intrinsic resistance of SLGNR, it is not suitable for on-chip interconnects [11]–[13]. Depending on the types of connection with surrounding devices or interconnects, MLGNR can be further classified into top contact MLGNR (TC-MLGNR) and side contact MLGNR (SC-MLGNR) [9], [14], [15]. In the former, only the top most layer is connected to other contacts, whereas all layers are coupled with the surrounding contacts in the latter. Hence the unique connection of SC-MLGNR enables it to have a smaller resistance when compared with TC-MLGNR. Therefore, SC-MLGNR is selected as the interconnect material in this work.

Although SC-MLGNR has a host of excellent electrical performance, there are still some limitation to be solved in the practical application on-chip interconnects. The SC-MLGNR is easy to be converted into graphite due to the interlayer electron hopping, which results in reducing its electron MFP and thereby increasing the distributed scattering resistance [16]. The reason for the interlayer electron hopping phenomenon is that the carbon-carbon bond lengths are modulated by the elastic strain of the stacked multiple layers [16], [17]. As a consequence, it is crucial to seek an alternative structure for enhancing the MFP of SC-MLGNR. Over the past few years, it is reported that the carrier mobility of GNR layers can be improved by inserting the high-k dielectric layer between two adjacent GNR layers, hence its MFP could be improved [16], [18]. This can restrict SC-MLGNR to turn into the graphite and improve the total number of graphene layers of SC-MLGNR interconnects. In [16], the number of graphene layers can reach 60 by inserting the HfO_2 dielectric between adjacent GNR layers at 22 nm technology node. Moreover, inserting the high-k dielectric layer in SC-MLGNR can also decrease the electron scattering rate of GNR and thus reduce the overall resistance of SC-MLGNR interconnects [19].

In order to fabricate the proposed interconnect structure, as shown in Fig. 1, which can be done by applying the atom layer deposition (ALD) technique. On the basis of the available literature, a series of dielectric materials could be grown on the graphene layer by using the well-developed technique. As reported in Refs. [20]–[22], the hexagonal

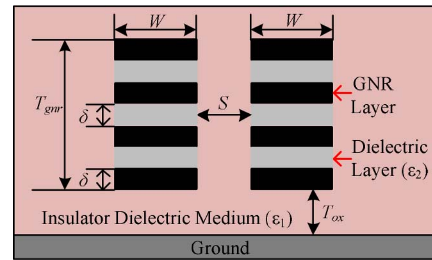

FIGURE 1. The schematic structure of two-line coupled MLGNR interconnects with a thin dielectric material (ε_2) inserted between adjacent GNR layers, and MLGNR interconnects surrounding the insulator dielectric medium (ε_1).

boron nitride h-BN, aluminum oxide Al_2O_3 and hafnium oxide HfO_2 have been deposited on graphene layer by using ALD technique. The advantage of using the ALD technique can achieve the precise control of the film thickness and uniformity [16].

In view of the interconnect width scaling down to the nanometer order at the end of the roadmap, the propagation delay and transfer gain of global level interconnects in VLSI circuits have become paramount consideration factors due to the longer interconnect distance. In the past few years, a multitude of studies with respect to these issues on MLGNR interconnect system have been done. In [23], [24], Kaur *et al.* and Bhattacharya *et al.* investigated the propagation delay of MLGNR interconnect system. In [15], [25], [26], the propagation delay and power dissipation for the single-line of MLGNR interconnect are analyzed. In [8], [27], [28], the model of propagation delay and transfer gain of MLGNR interconnect are presented. However, the works mentioned above are only focused on establishing the mathematical model, while the optimization method for reducing the propagation delay and enhancing the transfer gain of on-chip MLGNR interconnects is not proposed. Accordingly, it is urgent to seek a new technology to further improve the MLGNR interconnect performance in the VLSI circuits at the end of the roadmap. In our previous paper [6], the ultra-low-k dielectric material (nanoglass) replacing the traditional SiO_2 dielectric medium in coupled MLGNR interconnects to reduce the propagation delay and crosstalk noise and to enhance the transfer gain is proposed. Meanwhile, in [16], [19], it is reported that inserting the high-k dielectric (HfO_2) material between adjacent GNR layers in SC-MLGNR interconnect can reduce the propagation delay, crosstalk noise and energy-delay-product. Therefore, we propose a new technology of collaborative applying the ultra-low-k dielectric material (nanoglass) and the high-k dielectric material (HfO_2) in coupled multilayer graphene nanoribbon (MLGNR) interconnects to further improve the performance of propagation delay and transfer gain of on-chip interconnect in this paper.

To the best of our knowledge, it can be found that most literatures concerning the SC-MLGNR interconnects are only investigated on the performance parameters in

the time domain. Apparently, there is no doubt that the performance parameter of SC-MLGNR interconnects in the frequency domain is also the extremely significant consideration factor for providing the guideline to design the on-chip interconnect in VLSI circuits. Bandwidth denotes the capability of data transmitting for a system, which plays a vital role in an on-chip interconnect system [29], [30]. For an on-chip interconnect system, a larger bandwidth can remarkable reduce the total time to convey a certain number of data [2], [31]. However, so far the study regarding the 3-dB bandwidth of the SC-MLGNR interconnects is still rare. Based on the aforementioned discussion, besides the propagation delay and transfer gain, a mathematical model for 3-dB bandwidth of the SC-MLGNR interconnects by replacing the conventional SC-MLGNR structure with the proposed new technology is also presented in this paper.

II. ELECTRICAL MODELING OF MLGNR INTERCONNECTS

A. TWO-LINE COUPLED MLGNR INTERCONNECT

A typical schematic structure of two-line coupled MLGNR interconnects placed above the ground plane at a distance T_{ox} is depicted in Fig. 1. Here W, S, T_{gnr}, T_{ox}, ε_1 and ε_2 are line width, line space, line height, thickness of the insulator dielectric medium, relative dielectric constant of the insulator dielectric medium and relative dielectric constant of interlayer dielectric material between two adjacent GNR layers, respectively. Here the common SiO_2 (i.e., $\varepsilon_1 = 3.9$) insulator dielectric medium can be replaced by the ultra-low-k dielectric material, such as the nanoglass (i.e., $\varepsilon_1 = 1.3$), to obtain a better interconnect performance as reported in [6]. In addition, here the conventional (pristine) MLGNR by inserting the high-k dielectric material (HfO_2) between successive GNR layers can also improve the performance of MLGNR interconnects. For the conventional MLGNR, the gap between two adjacent GNR layers is not filled with the high-k dielectric material and can be regarded as a vacuum layer (i.e., $\varepsilon_2 = 1$). In this work, we investigated the effect of the MLGNR by inserting the hafnium oxide HfO_2 (i.e., $\varepsilon_2 = 25$) between two adjacent GNR layers on the performance of MLGNR interconnect. The total number of layers for MLGNR interconnect is dependent on the line height T_{gnr} and can be calculated as $N_{layer} = \text{Integer}[T_{gnr}/2\delta + 1/2]$. Wherein the operator Integer[.] denotes that only the integer part for a decimal is considered. The thicknesses of each GNR layer and the separation distance between adjacent GNR layers are all δ (=0.34nm) [16], [26].

An equivalent distributed circuit model of two-line coupled MLGNR interconnects with driver resistance R_D, driver capacitance C_D and load capacitance C_L for aggressor and victim lines is shown in Fig. 2, where the coupled MLGNR interconnects is composed of lumped and distributed parts.

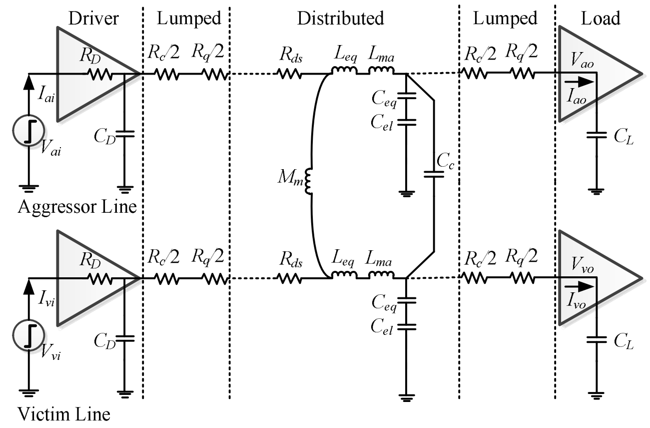

FIGURE 2. The equivalent distributed circuit model of two-line coupled MLGNR interconnects with the drivers and loads.

As exhibited in Fig. 2, R_{lu} and R_{ds} are the lumped resistance and per unit length (p.u.l.) distributed scattering resistance, respectively. The lumped resistance R_{lu} is comprised of quantum resistance R_q and nonideal contact resistance R_c, where they are equally arranged at two symmetrical ports of the equivalent circuit. The distributed scattering resistance R_{ds} exists only when the interconnect length L_{gnr} is larger than the effective mean free path (MFP) λ_{eff}. They can be expressed as [32],

$$R_{lu} = R_c + R_q = \frac{R_{cm}}{N_{layer} \cdot N_{ch}} + \frac{R_{qm}}{N_{layer} \cdot N_{ch}}, \tag{1}$$

$$R_{ds} = \begin{cases} \frac{R_{qm}}{N_{layer} \cdot N_{ch} \cdot \lambda_{eff}} & L_{gnr} > \lambda_{eff} \\ 0 & L_{gnr} < \lambda_{eff}. \end{cases} \tag{2}$$

Here, R_{cm} represents the monolayer nonideal contact resistance and its value is in the range from 1 KΩ to 20 KΩ [33]. R_{qm} denotes the monolayer quantum resistance and can be written as $R_{qm} = h/2e^2$ (herein h is Plank's constant and e is electron charge). N_{ch} is the total number of conducting channels of monolayer GNR and can be computed by [29], [34],

$$N_{ch} = a_0 + a_1 \cdot W + a_2 \cdot W^2 + a_3 \cdot E_f + a_4 \cdot E_f \cdot W + a_5 \cdot E_f^2. \tag{3}$$

wherein a_0 to a_5 represent the parameters for zigzag MLGNR (zz-MLGNR) under the room temperature (300K) when the value of Fermi energy E_f is greater than 0 [34]. Owing to the total number of conducting channels of zigzag MLGNR (zz-MLGNR) exceeding the armchair MLGNR (ac-MLGNR), hence the zz-MLGNR interconnect possesses a smaller distributed scattering resistance when compared with ac-MLGNR interconnect. Therefore, only the zz-MLGNR as the interconnect material is discussed in this work. The mathematical expression of the MFP λ_{eff} of MLGNR interconnect with inserting the high-k dielectric material between adjacent GNR layers is given by [16], [19],

$$\lambda_{eff} = \tau v_f. \tag{4}$$

Herein τ and v_f are the scattering time and Fermi velocity of electrons in graphene ($= 8 \cdot 10^5$ m/s), respectively. The mathematical expression of scattering rate τ^{-1} of GNR with

a thin dielectric material inserted between adjacent GNR layers is deduced as below [19],

$$\tau^{-1} = 2v_f k_F \frac{n_i}{n_e} \int_0^{\pi} d\theta \times \left(\sin(\theta) \Big/ \left(\left(\pi + \frac{2\hbar v_f \varepsilon_2 \varepsilon_0}{e^2} \right) \sin\left(\frac{\theta}{2}\right) + 4 - \frac{2\pi}{3n_e} \left(\frac{k_B T}{\hbar v_f} \right)^2 \right) \right)^2 \quad (5)$$

where $k_F = (\pi n_e)^{0.5}$ denotes the Fermi momentum. n_i and n_e represent the impurity concentration and electron concentration in graphene, respectively [16]. $\hbar$, k_B and T are the reduced Planck's constant, Boltzmann's constant and reference temperature, respectively. ε_0 is the vacuum dielectric constant. Herein, in order to investigate the impact of high-k dielectric material on the performance of SC-MLGNR interconnects, the relative dielectric constant ε_2 is adopted to represent the different interlayer dielectric materials inserted between adjacent GNR layers in this work.

The total distributed capacitance C_T of MLGNR interconnects consists of the equivalent quantum capacitance C_{eq} and the electrostatic capacitance C_{el}, and their relationship can be expressed as Equation (6). The p.u.l. equivalent quantum capacitance C_{eq} can be solved by applying a recursive method as follows [11], [32], [35], [42],

$$C_T = \left(\frac{1}{C_{eq}} + \frac{1}{C_{el}} \right)^{-1}, \quad (6)$$

$$C_{rec}^1 = C_{mq} = \frac{4e^2 N_{ch}}{h v_f}, \quad (7)$$

$$C_{rec}^i = \left(\frac{1}{C_{rec}^{i-1}} + \frac{1}{C_m} \right)^{-1} + C_{mq}, \quad (8)$$

$$C_{eq} = C_{rec}^{N_{layer}}. \quad (9)$$

Here C_{mq} represents the p.u.l. quantum capacitance of monolayer GNR. C_m denotes the p.u.l. coupling capacitance between adjacent GNR layers and can be written as $C_m = \varepsilon_2 \varepsilon_0 W/\delta$. Similarly, for analyzing the effect of the ultra-low-k dielectric material on the performance of SC-MLGNR interconnects, the relative dielectric constant ε_1 is introduced to distinguish different insulator dielectric mediums in this paper. The p.u.l. electrostatic capacitance C_{el} is contributed by the interconnect dimension and relative dielectric constant ε_1 of insulator dielectric medium, which can be expressed as [25],

$$C_{el} = \varepsilon_1 \cdot \varepsilon_0 \cdot M\left[\tanh\left(\frac{\pi \cdot W}{4 \cdot T_{ox}} \right) \right]. \quad (10)$$

wherein M [.] can be defined as [36],

$$M[\gamma] = \begin{cases} \dfrac{2\cdot\pi}{\ln\left(\left(2+2\cdot\sqrt[4]{1-\gamma^2}\right)/\left(1-\sqrt[4]{1-\gamma^2}\right)\right)}, & 0 \le \gamma \le \frac{1}{\sqrt{2}} \\ \frac{2}{\pi} \cdot \ln\left(\frac{2+2\cdot\sqrt{\gamma}}{1-\sqrt{\gamma}}\right), & \frac{1}{\sqrt{2}} \le \gamma \le 1. \end{cases} \quad (11)$$

The total distributed inductance L_T of MLGNR interconnects includes the equivalent kinetic inductance L_{eq} and magnetic inductance L_{ma}. Being similar to the situation of the equivalent quantum capacitance C_{eq}, the p.u.l. equivalent kinetic inductance L_{eq} also can be obtained by using a recursive scheme as below [11], [35], [42],

$$L_{rec}^1 = L_k = h/4e^2 v_f N_{ch}, \quad (12)$$

$$L_{rec}^i = \left(\frac{1}{L_{rec}^{i-1} + L_m} + \frac{1}{L_k} \right)^{-1}, \quad (13)$$

$$L_{eq} = L_{rec}^{N_{layer}}. \quad (14)$$

Here, L_k is the p.u.l. kinetic inductance of monolayer GNR. L_m represents the p.u.l. coupling inductance between adjacent GNR layers and can be calculated as $L_m = \mu_0 \delta/W$ (here $\mu_0 = 8.854 \cdot 10^{-12}$ is the vacuum magnetic permeability). Therefore, the total distributed inductance L_T of MLGNR interconnect can be illustrated as,

$$L_T = L_{eq} + L_{ma} = L_{eq} + \frac{\mu_0 T_{ox}}{W}. \quad (15)$$

As displayed in Fig. 2, the effects of coupling capacitance C_c and mutual inductance M_m on the dynamic crosstalk of the coupled MLGNR interconnects must be taken into account. The mathematical expressions of p.u.l. C_c and M_m are formulated as follows [6], [33],

$$C_c = \frac{0.5}{1 + \left(\frac{S}{(T_{gnr}+T_{ox})}\right)^2} \cdot C_{[BCP]}\left(\frac{T_{gnr}}{S/2}, \frac{2 \cdot T_{ox}}{S/2} \right) + \frac{0.87}{1 + \left(\frac{S/2}{(T_{gnr}+T_{ox})}\right)^2} \cdot C_{[CP]}\left(\frac{W}{S} \right), \quad (16)$$

$$M_m = \frac{\mu_0}{2\pi} \ln\left(\frac{2}{S+W} - 1 \right). \quad (17)$$

Here $C_{[BCP]}(x, y)$ and $C_{[CP]}(x)$ are defined as below,

$$C_{[BCP]}(x, y) = \frac{\varepsilon_1 \cdot \varepsilon_0}{2} \cdot M\left[K_{[BCP]}(x, y) \right], \quad (18)$$

$$C_{[CP]}(x) = \frac{\varepsilon_1 \cdot \varepsilon_0}{4} \cdot M\left[K_{[CP]}(x) \right]. \quad (19)$$

where the function M [.] is illustrated in Equation (11), $K_{[BCP]}(x, y)$ and $K_{[CP]}(x)$ are exhibited in [6], [36].

B. THREE-LINE COUPLED MLGNR INTERCONNECT

In the practice application, multiple line structure is more common in VLSI circuits. Therefore, the simple two-line coupled interconnects are not sufficient enough to validate the signal coupling crosstalk effects. For the sake of improving the generality of our model, this section also takes three-line coupled MLGNR interconnects into account, as shown in Fig. 4. And regarding RLC parameters can be obtained on the basis of aforementioned method.

III. CROSSTALK DELAY AND BANDWIDTH MODEL

In order to conveniently analyze the circuit model depicted in Fig. 2, the coupled-two identical interconnects can be divided into two independent line by applying the decoupling technique. The equivalent circuit model of the decoupled

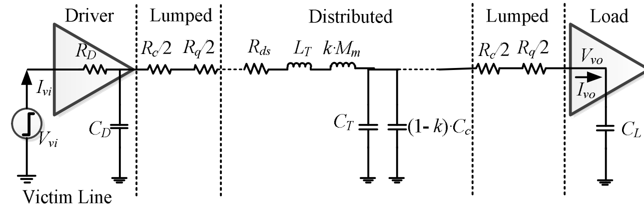

FIGURE 3. The equivalent distributed circuit model of the decoupled victim line by using the decoupling technique.

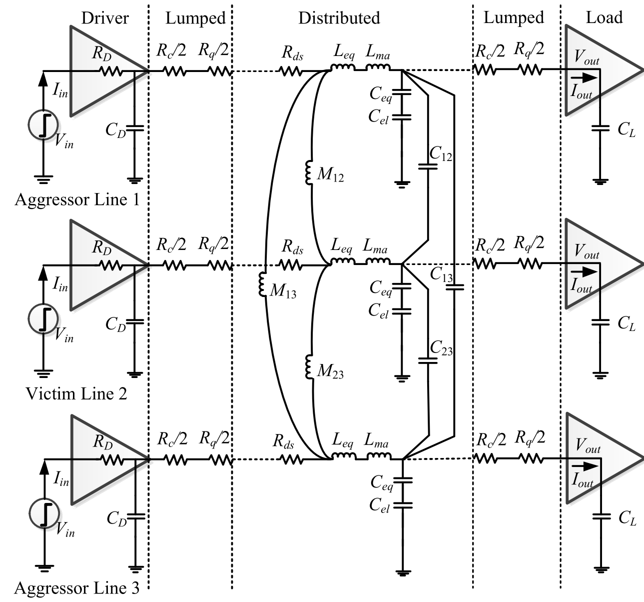

FIGURE 4. The equivalent distributed circuit model of three-line coupled MLGNR interconnects with the drivers and loads.

victim MLGNR line is shown in Fig. 3, where k is the switching factor that indicates the switching direction of input signals of two-line coupled MLGNR interconnects. The dynamic crosstalk includes in-phase crosstalk and out-of-phase crosstalk modes. For the switching factor k, $k = 1$ and $k = -1$ are defined to distinguish the corresponding crosstalk modes, that is the aggressor and victim MLGNR lines switching in the same direction and opposite direction at the same time, respectively.

Obviously, it is indispensable to study the coupled line structure over two-line because its interconnect crosstalk is more complex. Therefore, in this work, an equivalent circuit of three-line coupled MLGNR interconnects is presented as shown in Fig. 4. Here, we adopted the decoupling method presented in [40] to obtain its equivalent capacitance and inductance parameters. Based on the [40], each switching case can be symbolized as "↑" (i.e., switching from logic 0 to logic 1), "↓" (i.e., switching from logic 1 to logic 0) and "0" (i.e., the quiet state). All of the switching patterns for three-line coupled interconnects can be expressed as the linear combination of three fundamental switching modes (i.e., "↑↑↑", "↓↑0 (0 ↓↑)" and "↑ 0 ↓"). Take "↓↑↓" as an instance, it can be expressed as(↓↑↓) $= \frac{1}{3}\{$(↑↑↑) $+ 2$(↑↓ 0) $+ 2$(0 ↓↑)$\}$.

In order to investigate the step response, propagation delay, frequency response and bandwidth of coupled MLGNR interconnect, it is crucial to derive the transfer function of input-output interconnect system by applying the ABCD parameter matrix approach. As shown in Fig. 3, the total ABCD parameter matrix of the decoupled victim MLGNR line can be deduced as [6],

$$\begin{bmatrix} A_T & B_T \\ C_T & D_T \end{bmatrix} = \begin{bmatrix} 1 & R_D \\ 0 & 1 \end{bmatrix} \cdot \begin{bmatrix} 1 & 0 \\ sC_D & 1 \end{bmatrix} \cdot \begin{bmatrix} 1 & \frac{R_{lu}}{2} \\ 0 & 1 \end{bmatrix} \times \begin{bmatrix} \cosh(\theta L_{gnr}) & Z\sinh(\theta L_{gnr}) \\ \frac{\sinh(\theta L_{gnr})}{Z} & \cosh(\theta L_{gnr}) \end{bmatrix} \cdot \begin{bmatrix} 1 & \frac{R_{lu}}{2} \\ 0 & 1 \end{bmatrix}. \tag{20}$$

wherein θ and Z are the propagation constant and characteristic impedance of the decoupled victim MLGNR line and their mathematical expressions are exhibited in Equations (21) and (22), respectively. Due to the existing of coupling capacitance C_c and mutual inductance M_m, the total distributed capacitance C_E and total distributed inductance L_E of the decoupled victim MLGNR line can be rewritten as $C_E = C_T + (1-k)C_c$ and $L_E = L_T + kM_m$, respectively.

$$\theta = \sqrt{(R_{ds} + sL_E) \cdot sC_E}, \tag{21}$$

$$Z = \sqrt{\frac{R_{ds} + sL_E}{sC_E}}. \tag{22}$$

Based on the principle of ABCD matrix approach, input voltage can be expressed as a function of output voltage and output current. Hence, combining with the relationship of output current and output voltage of $I_{vo}(s) = sC_L \cdot V_{vo}(s)$, the transfer function of the decoupled victim MLGNR line is deduced as below,

$$H(s) = \frac{V_{vo}(s)}{V_{vi}(s)} = \frac{1}{A_T + sC_L B_T} = \frac{1}{1 + b_1 s + b_2 s^2 + b_3 s^3 + b_4 s^4}. \tag{23}$$

Here, the transfer function is adopted a fourth-order pade's expansion, which can obtain the signal integrity characteristics at the output port of the MLGNR interconnect system. The all coefficients for the Equation (23) can be listed as follows,

$$b_1 = \frac{1}{2}L_{gnr}^2 R_{ds} C_E + C_D R_D + C_L(R_{lu} + R_D) + L_{gnr} R_D C_E + \frac{1}{2}L_{gnr} R_{lu} C_E + L_{gnr} C_L R_{ds}, \tag{23a}$$

$$\begin{aligned} b_2 = &\frac{1}{24}L_{gnr}^4 R_{ds}^2 C_E^2 + \frac{1}{2}C_l(R_{lu} + R_D)L_{gnr}^2 C_E R_{ds} \\ &+ \frac{1}{6}L_{gnr}^3 C_E^2 R_{ds} R_D + \frac{1}{2}L_{gnr} C_D R_D R_{lu} C_E + C_D R_D R_{lu} C_L \\ &+ \frac{1}{12}L_{gnr}^3 C_E^2 R_{ds} R_{lu} + \frac{1}{6}L_{gnr}^3 C_E C_L R_{ds}^2 + L_{gnr} C_L L_E \\ &+ \frac{1}{2}L_{gnr}^2 C_E L_E + \frac{1}{4}L_{gnr} C_L R_{lu}^2 C_E + L_{gnr} C_L C_D R_{ds} R_D \\ &+ \frac{1}{2}L_{gnr} C_L R_D R_{lu} C_E + \frac{1}{2}C_D R_D L_{gnr}^2 C_E R_{ds}, \end{aligned} \tag{23b}$$

$$\begin{aligned}
b_3 = {} & C_L(R_{lu}+R_D)\left(\frac{1}{2}L_{gnr}^2C_EL_E+\frac{1}{24}L_{gnr}^4R_{ds}^2C_E^2\right) \\
&+\frac{1}{12}R_DR_{lu}C_LL_{gnr}^2R_{ds}C_DC_E\left(6+L_{gnr}C_E\right) \\
&+\frac{1}{240}L_{gnr}^5C_E^2R_{ds}^2(2C_ER_D+C_ER_{lu}+2C_LR_{ds}) \\
&+\frac{1}{24}C_DR_DL_{gnr}^2C_E\left(12L_E+L_{gnr}^2R_{ds}^2C_E\right) \\
&+\frac{1}{24}L_{gnr}^3C_E^2R_{ds}2L_{gnr}L_E+C_LR_{lu}^2 \\
&+L_{gnr}C_LL_E\left(\frac{1}{3}L_{gnr}^2C_ER_{ds}+C_DR_D\right)+\frac{1}{6}L_{gnr}^3C_E^2L_ER_D \\
&+\frac{1}{12}R_DR_{lu}C_LL_{gnr}^2R_{ds}L_{gnr}C_E^2+\frac{1}{4}L_{gnr}C_LC_DR_DR_{lu}^2C_E \\
&+\frac{1}{720}L_{gnr}^6R_{ds}^3C_E^3+\frac{1}{12}L_{gnr}^3C_E^2L_ER_{lu}, \qquad (23c)
\end{aligned}$$

$$\begin{aligned}
b_4 = {} & \frac{1}{120}L_{gnr}^5C_E^2L_ER_{ds}(C_ER_{lu}+3C_LR_{ds}) \\
&+\left(C_DR_D+C_L(R_{lu}+R_D)\frac{1}{12}L_{gnr}^4R_{ds}L_EC_E^2\right. \\
&+C_DR_DR_{lu}C_L\frac{1}{24}L_{gnr}^2C_E12L_E+L_{gnr}^2R_{ds}^2C_E \\
&+\frac{1}{10080}L_{gnr}^7C_E^3R_{ds}^3(2C_ER_D+C_ER_{lu}+2C_LR_{ds}) \\
&+\frac{1}{480}L_{gnr}^5C_E^3R_{ds}\left(C_LR_{ds}R_{lu}^2+8L_ER_D\right)+\frac{1}{6}L_{gnr}^3C_EC_LL_E^2 \\
&+\frac{1}{24}L_{gnr}^3C_EC_L\left(C_EL_ER_{lu}^2+C_DR_DR_{ds}C_ER_{lu}^2+8L_E\right) \\
&+\frac{1}{240}L_{gnr}^5C_E^2R_{ds}^2R_D(C_EC_LR_{lu}+C_EC_DR_{lu}+2C_LC_DR_{ds}) \\
&+\frac{1}{12}L_{gnr}^3C_E^2L_ER_DR_{lu}(C_L+C_D)+\frac{1}{40320}L_{gnr}^8R_{ds}^4C_E^4 \\
&+\frac{1}{240}L_{gnr}^4L_EC_E^2\left(10L_E+L_{gnr}^2R_{ds}^2C_E\right) \\
&+\frac{1}{720}L_{gnr}^6R_{ds}^3C_E^6(C_DR_D+C_L(R_{lu}+R_D). \qquad (23d)
\end{aligned}$$

Step response represents the transient response of the output port for an interconnect system that is triggered by a unit step signal of the input port. It indicates the time domain performance of the output voltage signal for an interconnect system when the input voltage signal changes from logic "0" to logic "1" in a very short time. Certainly, step response can be used to evaluate the stability of an interconnect system. Here, the input voltage signal $V_{in}(s) = 1/s$ is selected as the ideal step-signal in this work. Therefore the step response of victim MLGNR interconnect in the Laplace domain can be expressed as,

$$V_{out}(s) = \frac{V_{in}(s)}{1+b_1s+b_2s^2+b_3s^3+b_4s^4}. \qquad (24)$$

Subsequently, we can obtain the step response $V_{out}(t)$ at the time domain by applying the inverse Laplace transform for the Equation (24). In addition, the 50% propagation delay of victim MLGNR line in different phase modes can be got according to the numerical simulation data by carrying out the analytical expressions of step response $V_{out}(t)$ as below,

$$V_{out}(t) = L\left[\frac{V_{in}(s)}{1+b_1s+b_2s^2+b_3s^3+b_4s^4}\right]^{-1}. \qquad (25)$$

In the frequency domain, there is no doubt that the transfer gain and bandwidth are regarded as the indispensable frequency parameters to analyze the behavior of the coupled MLGNR transmission system. We used the $s = j2\pi f$ into Equation (23) to derive the mathematical expression concerning the magnitude of transfer gain, which is formulated as,

$$|T_{tran}(f)| = \begin{pmatrix} \left(1-b_2(2\pi f)^2+b_4(2\pi f)^4\right)^2 \\ +\left(b_12\pi f-b_3(2\pi f)^3\right)^2 \end{pmatrix}^{-0.5}. \qquad (26)$$

In view of the coupled driver-MLGNR interconnect-load system shown in Fig. 3 can be considered as a RC low pass filter, thus it can deduce a cut-off frequency. For any signal transmission system, the bandwidth is usually expressed in the 3-dB bandwidth $f_{3\text{dB}}$. In the light of the definition of 3-dB bandwidth, the 3-dB bandwidth is equivalent to the cut-off frequency in which the magnitude of transfer gain of interconnect system cuts down $1/\sqrt{2}$. Based on the discussion mentioned above, we proposed a mathematical expression to obtain accurately the 3-dB bandwidth $f_{3\text{dB}}$ as follows,

$$\begin{aligned} c_4(2\pi f_{3dB})^8+c_3(2\pi f_{3dB})^6+c_2(2\pi f_{3dB})^4 \\ +c_1(2\pi f_{3dB})^2-1=0. \qquad (27) \end{aligned}$$

where each coefficient of Equation (27) is expressed as below,

$$c_4 = b_4^2 \qquad (27a)$$
$$c_3 = -2b_2b_4+b_3^2 \qquad (27b)$$
$$c_2 = 2b_4-2b_1b_3+b_2^2 \qquad (27c)$$
$$c_1 = -2b_2+b_1^2. \qquad (27d)$$

IV. RESULTS AND DISCUSSIONS

This section will analyze the impacts of the ultra-k dielectric and high-k dielectric materials on step response, crosstalk delay, transfer gain and 3-dB bandwidth of coupled MLGNR interconnects at 7 nm technology node of global level. In this work, we proposed a new scheme of collaborative using the ultra-low-k dielectric and the high-k dielectric materials in coupled MLGNR interconnects. In order to demonstrate the superiority of this proposed method, we defined the four cases as follows,

Case 1: The conventional MLGNR interconnects (The insulator dielectric medium is selected as SiO_2, and the gap between two adjacent GNR layers is separated by a vacuum layer, i.e., $\varepsilon_1 = 3.9$, $\varepsilon_2 = 1$).

Case 2: Only the insulator dielectric medium $SiO_2$is replaced with the nanoglass of ultra-low-k dielectric material, and the gap between two adjacent GNR layers is also separated by a vacuum layer (i.e., $\varepsilon_1 = 1.3$, $\varepsilon_2 = 1$).

Case 3: Only the gap between two adjacent GNR layers is inserted with the hafnium oxide HfO_2 of high-k dielectric material, and the insulator dielectric medium is set as SiO_2 (i.e., $\varepsilon_1 = 3.9$, $\varepsilon_2 = 25$).

Case 4: The proposed new method of collaborative using the ultra-low-k dielectric and the high-k dielectric materials in the coupled MLGNR interconnects (The insulator dielectric medium is replaced with the nanoglass of ultra-low-k dielectric material, and the gap between two adjacent GNR layers is inserted with the hafnium oxide HfO_2 of high-k dielectric material, i.e., $\varepsilon_1 = 1.3$, $\varepsilon_2 = 25$).

The geometrical and physical parameters are extracted from [3], [37] as follows, $W = 11.5$ nm, $T_{gnr} = 26.91$ nm, $S = 11.5$ nm, $T_{ox} = 17.25$ nm, $E_f = 0.3$ eV, $\varepsilon_0 = 8.854 \cdot 10^{-12}$ F/m, $\mu_0 = 4\pi \cdot 10^{-7}$, $n_i = 2 \times 10^{15}$ m^{-2}, $n_e = 8 \times 10^{16}$ m^{-2}, $T = 300$K, $R_D = 20.51$ kΩ, $C_D = 0.063$ fF, $C_L = 0.2$ fF. Herein R_D, C_D and C_L represent the equivalent values of minimum-sized gate. For the global level interconnects ($100\mu m \leq L_{gnr} \leq 10mm$) [38], the sizes of driver and load are usually 100 times greater than that of the minimum-size gate [6], then their values can be redefined as, $R'_D = R_D/100$, $C'_D = C_D \cdot 100$ and $C'_L = C_L \cdot 100$. In this work, all the numerical simulation results presented in the following section are obtained by using the MATLAB R2013a. In addition, it is essential that the proposed results should be compared with the state-of-the-art literature. To the best of our knowledge, so far only the [16], [19] have investigated regarding the inserting high-k dielectric material between adjacent GNR layers in MLGNR interconnects. The [19] presented a new technique of unconditionally stable finite-difference time-domain (USFDTD) approach to analyze the propagation delay, step response and so on, which can overcome the limitations of the conventional finite-difference time-domain (FDTD). Therefore, the results obtained by the proposed model are validated with [19] in this paper.

A. MEAN FREE PATH OF MLGNR INTERCONNECT

It is evidently that the mean free path (MFP) of MLGNR is strongly dependent on the impurity concentration n_i of interlayer dielectric and the relative dielectric constant $\varepsilon_2$of interlayer dielectric according to Equations (4) and (5). As reported in [16], the value of impurity concentration n_i is determined by the quality of dielectric layer. The cleaner dielectric sample can lead to a smaller impurity concentration ($n_i = 0.2 \cdot 10^{16}$ m^{-2}) whereas the dirty dielectric sample will result in a larger impurity concentration ($n_i = 3.5 \cdot 10^{16}$ m^{-2}) [41]. The charged impurities are existing in both the inside of dielectric material and the grapheme-dielectric interface. Moreover, the relative dielectric constant ε_2 in each GNR layer is determined by its surrounding media. When the GNR layer is sandwiched between two different dielectric (ε_a and ε_b), then the relative dielectric constant ε_2 of GNR should be redefined as $\varepsilon_2 = (\varepsilon_a + \varepsilon_b)/2$ [19]. Based on the available literature, typical dielectric can be used as the interlayer dielectric materials that include silicon oxide SiO_2, aluminum oxide Al_2O_3 and hafnium oxide HfO_2 [16].

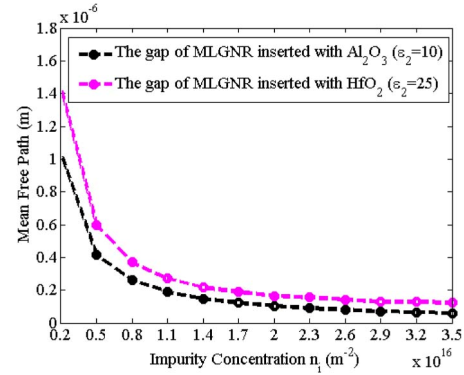

FIGURE 5. **The mean free path of MLGNR versus impurity concentration n_i.**

The mean free path of GNR versus impurity concentration for different interlayer dielectric materials is exhibited in Fig. 5. Herein the gap of between two adjacent GNR layers is inserted with the Al_2O_3 and HfO_2, respectively. As described in Fig. 5, it can be seen that the MFP decreases with the increase of impurity concentration n_i for inserting Al_2O_3 and HfO_2 cases. Here the MFP of GNR with the cleaner dielectric for inserting Al_2O_3 and HfO_2 cases are 17.50 and 11.77 times larger than that with the dirty dielectric, respectively. In addition, it is found from Fig. 5 that the MFP of GNR by inserting HfO_2 is greater than that of inserting Al_2O_3 case. Therefore, reducing the impurity concentration and applying the high-k dielectric material between adjacent GNR layers are the effective method to improve the MFP of MLGNR interconnects.

B. TWO-LINE COUPLED MLGNR INTERCONNECT MODEL

In order to investigate the superiority of the proposed new method of collaborative using the ultra-low-k dielectric and the high-k dielectric materials in two-line coupled MLGNR interconnects (i.e., case 4), the step response of victim MLGNR line with interconnect length $L_{gnr} = 1000$ μm for the defined four cases under in-phase and out-of-phase crosstalk modes is displayed in Fig. 6(a) and 6(b), respectively.

Fig. 6(a) and 6(b) show that the output voltages in all circumstances will take a period of time to reach the steady-state value 1 V. As described in Fig. 6(a) and 6(b), it is observed that the time of reaching the steady-state value of the case 2, case 3 and case 4 are all lesser than that of the case 1 for in-phase and out-of-phase crosstalk modes. Furthermore, it can be found that the time of reaching the steady-state value of the proposed case 4 is obviously lower than that of all other cases for in-phase and out-of-phase crosstalk modes. The reason for the time of reaching the steady-state value of the case 2 lesser than case 1 is that the electrostatic capacitance C_{el} and coupling capacitance C_c will decrease as the relative dielectric constant ε_1 decreases, thereby, leading to a smaller total distributed capacitance C_T

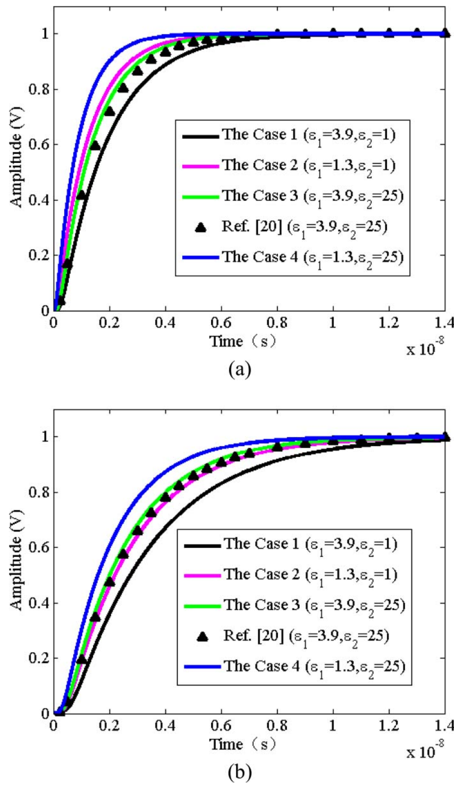

FIGURE 6. The step response of victim line of two-line coupled MLGNR interconnects with length $L_{gnr} = 1000$ μm for the defined four cases under in-phase crosstalk (a) and out-of-phase crosstalk (b) modes.

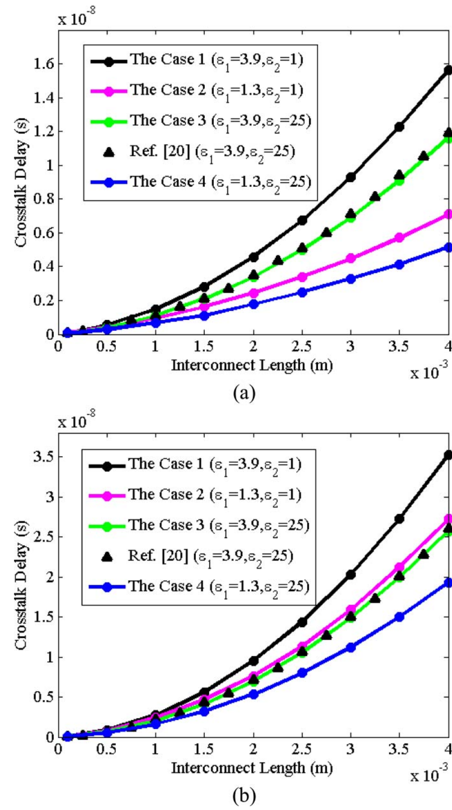

FIGURE 7. The 50% propagation delay of victim line of two-line coupled MLGNR interconnects with different length for the defined four cases under in-phase crosstalk (a) and out-of-phase crosstalk (b) modes.

of case 2 according to the Equations (6) (10) and (16). As a consequence, it can lead to the faster charging and discharging of parasitic capacitances. Thus case 2 has a lesser time of reaching the steady-state value than case 1. The corresponding reason for the time of reaching the steady-state value of the case 3 lesser than case 1 is that the effective mean free path λ_{eff} will increase as the relative dielectric constant ε_2 increases, thus give rise to a smaller distributed scattering resistance R_{ds} of case 3 combining with the Equations (2), (4) and (5). In addition, the time of reaching the steady-state value of the proposed case 4 lower than all other cases is because the case 4 combines the advantages of the case 2 and case 3. The proposed case 4 is a new technology of collaborative applying the ultra-low-k dielectric and the high-k dielectric materials in coupled MLGNR interconnects (i.e., case 4), which can reduce the electrostatic capacitance C_{el}, coupling capacitance C_c and distributed scattering resistance R_{ds} to reduce the time of reaching the steady-state value. Hence, this can lead to a lesser propagation delay for the proposed case 4.

Moreover, it can be found from Fig. 6 that the results of step response for the defined case 3 are in good accordance with the results of [19] under in-phase and out-of-phase crosstalk modes. The maximum relative errors between the defined case 3 and the [19] are 3.28% and 3.63% respectively for in-phase and out-of-phase crosstalk modes. The reason for this phenomenon is that they have the same relative dielectric constant (ε_1) of the insulator dielectric medium and relative dielectric constant (ε_2) of interlayer dielectric material between two adjacent GNR layers.

In order to further evaluate the time of reaching the steady-state value of the output voltage, it is significant to investigate 50% propagation delay under various conditions. The 50% propagation delay is defined as the time when the amplitude of step response $V_{out}(t)$ rises from 0 to half of its steady state value 1 V, which is the paramount parameter of the on-chip interconnect performance in the time domain. The corresponding results of the defined four cases on the 50% propagation delay of victim MLGNR line with different interconnect length under different phase modes are plotted in Fig. 7(a) and 7(b), respectively.

As shown in Fig. 7, it is also obvious that the propagation delay of the case 2, case 3 and case 4 are all lower than that of the case 1 for all phase crosstalk modes. Meanwhile, it can be seen that the propagation delay of the proposed case 4 is clearly lesser than that of all other cases for all phase crosstalk modes. Taking the interconnect length of $L_{gnr} = 3000$ μm as an instance, the delay time under out-of-phase crosstalk mode for the conventional MLGNR interconnects (case 1) is 20.311 ns while for case 2, case 3 and case 4 are 15.504 ns, 14.850 ns and 11.221 ns, respectively. Here the delay time for the conventional MLGNR

interconnects (case 1) is approximately twice greater than that the proposed case 4. Similarly, the delay time under in-phase crosstalk mode for case 1, case 2, case 3 and case 4 are 9.284 ns, 4.477 ns, 6.883 ns and 3.254 ns in the same length as the former, respectively. Wherein, the delay time for the proposed case 4 is nearly a third of the conventional MLGNR interconnects (case 1). The reason behind this is that the propagation delay is in positive proportion with the time of reaching the steady-state value 1 V mentioned above. In the light of the discussion mentioned above, the proposed case 4 has a lesser total distributed capacitance C_T and a smaller distributed scattering resistance R_{ds} compared with the conventional case 1. In addition, based on our numerical simulation results, the maximum reduction of delay time between the proposed case 4 and the conventional case 1 can reach to 15.911 ns for an interconnect length of $L_{gnr} = 4000\mu$m at the out-of-phase crosstalk mode. Therefore, the proposed method of collaborative using the ultra-low-k dielectric and the high-k dielectric materials in the MLGNR interconnects (i.e., case 4) can be regarded as a new promising technology to reduce the propagation delay of the coupled MLGNR interconnect system in VLSI circuits.

Moreover, it is remarkable from Fig. 7 that the propagation delay of victim MLGNR line under out-of-phase mode is higher than that under in-phase crosstalk mode at the same case. Giving the interconnect length of $L_{gnr} = 3500$ µm as an example, the delay time for case 1 under in-phase and out-of-phase modes are 12.251 ns and 27.250 ns. The corresponding values for case 2 are 5.712 ns and 20.710 ns, another situation for case 3 are 9.088 ns and 19.922 ns, and the last situation for the proposed case 4 are 4.152 ns and 14.986 ns. This is due to the fact that the Miller coupling capacitance $2C_c$ exists only in out-of-phase crosstalk mode, which results in that the total distributed capacitance C_T of the victim MLGNR line under in-phase mode is smaller than that under out-of-phase crosstalk mode. In addition, it can be seen from Fig. 7 that the delay results of the defined case 3 are in good matching with the results of [19] with the maximum relative error of 3.75% for any phase crosstalk mode.

The frequency response of victim MLGNR line with the interconnect length $L_{gnr} = 1000$ µm for the defined four cases under in-phase and out-of-phase crosstalk modes is illustrated in Fig. 8(a) and 8(b), respectively. Transfer gain is defined as the magnitude of frequency response of the interconnect system and represents the ratio of amplitude between the output and input signal versus different frequencies. The transfer gain of victim MLGNR line under in-phase and out-of-phase crosstalk modes can be solved by the Equation (26).

As described in Fig. 8, in high frequency region, it is clearly shown that the transfer gain of the case 2, case 3 and case 4 are evidently greater than that of the case 1 for different phase crosstalk modes. Besides, the transfer gain of the proposed case 4 is clearly larger than the case 1,

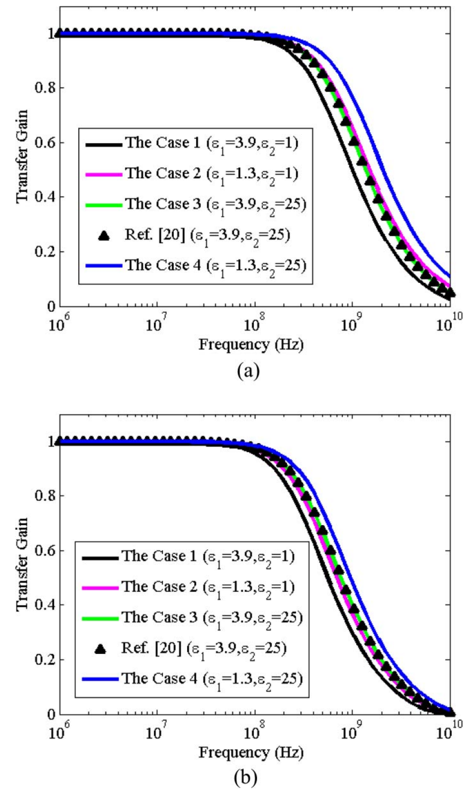

FIGURE 8. The frequency response of victim line of two-line coupled MLGNR interconnects with length $L_{gnr} = 1000$ µm for the defined four cases under in-phase crosstalk (a) and out-of-phase crosstalk (b) modes.

case 2 and case 3 for different phase crosstalk modes. It can be explained that the decoupled MLGNR interconnect system as depicted in Fig. 3 can be regarded as a RC low pass filter and its cut-off frequency can be approximately defined as: $1/(2\pi C_E R_{ds} L_{gnr}^2)$ [39], [42]. Based on the aforementioned discussion, it can be obtained that the case 2 can only reduce the electrostatic capacitance C_{el} and coupling capacitance C_c of the conventional MLGNR interconnect (case 1), the case 3 can only reduce the distributed scattering resistance R_{ds} of the traditional case 1. Whereas the proposed case 4 can reduce the electrostatic capacitance C_{el}, coupling capacitance C_c and distributed scattering resistance R_{ds} of the conventional case 1. Consequently, the victim MLGNR line for using the proposed case 4 has a larger cut-off frequency compared with the case 1, case 2 and case 3.

Moreover, it can be observed from Fig. 8 that the transfer gain of victim MLGNR line under out-of-phase mode is apparently lower than that under in-phase crosstalk mode at the same case. This is due to the fact that the total distributed capacitance C_T of the victim MLGNR line under in-phase mode is lesser than that of out-of-phase crosstalk mode. Certainly, the former will have a larger cut-off frequency compared with the latter. Furthermore, as depicted in Fig. 8, it is observed the results of frequency response for the defined case 3 are fairly consistent with the results of [19]

under in-phase and out-of-phase crosstalk modes. The maximum relative errors involved in the defined case 3 and the [19] for in-phase and out-of-phase crosstalk modes are 3.67% and 3.81%, respectively.

Besides the transfer gain, the bandwidth is also considered as the significant parameter to describe the interconnect performance in the frequency domain. Bandwidth represents the capability of data transmission, thus a larger bandwidth can effectively reduce the total time to transmit a certain amount of data from the input port to output port for the interconnect system [2], [31]. Hence, it is crucial to seek a new promising technology to expand the bandwidth of the MLGNR interconnect system. Accordingly, we investigated the superiority of the proposed case 4 on the 3-dB bandwidth of the victim MLGNR line in this work. Combining with the Equation (27), the corresponding results of the defined four cases on 3-dB bandwidth of victim MLGNR line with different interconnect length under in-phase and out-of-phase crosstalk modes are shown in Table 1.

As exhibited in Table 1, it is suggested that the 3-dB bandwidth of the case 2, case 3 and case 4 are all greater than that of the case 1 for in-phase and out-of-phase crosstalk modes. In the meantime, it can be also observed that the 3-dB bandwidth of the proposed case 4 is obviously higher than that of all other cases for in-phase and out-of-phase crosstalk modes. Using the interconnect length of $L_{gnr} = 3000\ \mu\text{m}$ under in-phase crosstalk mode as an example, the 3-dB bandwidth for case 2 is 2.022 times larger than that of the case 1. The corresponding value for case 3 is 1.350 times larger than that of the case 1. Whereas, another situation for case 4 is 2.784 times larger than that of the case 1. Based on the aforementioned discussion, the reason for this phenomenon is that applying the proposed case 4 has a larger cut-off frequency compared with the case 1, case 2 and case 3.

Furthermore, it is indicated from Table 1 that the 3-dB bandwidth of victim MLGNR line under in-phase mode is apparently greater than that under out-of-phase crosstalk mode at the same case. Giving the interconnect length of $L_{gnr} = 2000\ \mu\text{m}$ as an instance, the 3-dB bandwidth for case 1 under in-phase and out-of-phase crosstalk mode are 30.306 MHz and 14.762 MHz. The corresponding values for case 2 are 55.020 MHz and 19.028 MHz, another situation for case 3 are 41.004 MHz and 20.201 MHz, and the last situation for case 4 are 75.836 MHz and 26.292 MHz. This can be explained that the in-phase crosstalk mode has a larger cut-off frequency compared with the out-of-phase crosstalk mode at the same case. In addition, according to the data of Table 1, it is implied that the 3-dB bandwidth under in-phase crosstalk mode for the proposed case 4 can be expanded over 2.978 times than that of the conventional case 1 for an interconnect length of $L_{gnr} = 4000\mu\text{m}$. Meanwhile, it can be inferred that the 3-dB bandwidth under out-of-phase crosstalk mode for the proposed case 4 can be enhanced exceeding 1.824 times than that of the conventional case 1 in the same length as the former. Therefore, the proposed case 4 can be as a new prospective technology for the global level interconnects that has a significant application prospect in improving the bandwidth of interconnect system in VLSI circuits.

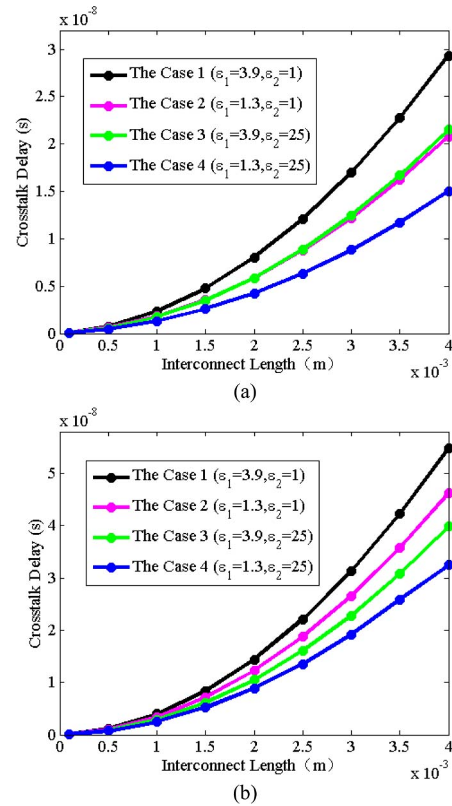

FIGURE 9. The 50% propagation delay of center line of three-line coupled MLGNR interconnects with different length for the defined four cases under in-phase crosstalk (a) and out-of-phase crosstalk (b) modes.

C. THREE-LINE COUPLED MLGNR INTERCONNECT MODEL

In view of the length of this paper, only the in-phase mode "↑↑↑" and out-of-phase mode "↓↑↓" for three-line coupled MLGNR interconnects are investigated in this work. In order to study the largest effect of the aggressor line on the victim line, the performance of center line (i.e., victim line 2 of Fig. 4) is focused. The propagation delay of center line of three-line coupled MLGNR interconnects with different length for the defined four cases under in-phase crosstalk and out-of-phase crosstalk modes is depicted in Fig. 9(a) and 9(b), respectively.

Being similar to the situation of two-line coupled MLGNR interconnects, it is observed from Fig. 9(a) and 9(b) that the propagation delay of the case 2, case 3 and case 4 are all lesser than that of the case 1 for in-phase and out-of-phase crosstalk modes. Meanwhile, it is found that the propagation delay of the proposed case 4 is evidently lower than that of all other cases for all phase crosstalk modes. In addition, combining with Fig. 7(a) and 7(b), it can be seen that the three-line coupled MLGNR interconnects have

TABLE 1. **The bandwidth of victim line of two-line coupled MLGNR interconnect with different length for the defined four cases under in-phase crosstalk and out-of-phase crosstalk modes.**

Length (μm)	3-dB bandwidth (MHz)							
	In-phase crosstalk mode				Out-of-phase crosstalk mode			
	Case 1	Case 2	Case 3	Case 4	Case 1	Case 2	Case 3	Case 4
100	1584.942	1677.410	2152.166	2286.645	1397.969	1474.015	1891.543	2001.223
200	750.932	836.271	1025.526	1148.930	601.050	659.220	819.264	902.862
400	328.032	400.504	447.996	552.101	227.384	263.050	310.815	361.908
600	192.244	253.972	262.099	350.371	120.881	144.518	165.340	199.155
800	128.169	181.108	174.447	249.887	75.198	91.892	102.878	126.744
1000	92.118	137.885	125.197	190.237	51.338	63.716	70.243	87.931
1500	48.806	81.727	66.153	112.706	25.006	31.791	34.217	43.908
2000	30.306	55.020	41.004	75.836	14.762	19.028	20.201	26.292
3000	15.001	30.328	20.250	41.765	6.898	9.027	9.441	12.478
4000	8.937	19.341	12.049	26.616	3.981	5.252	5.448	7.262

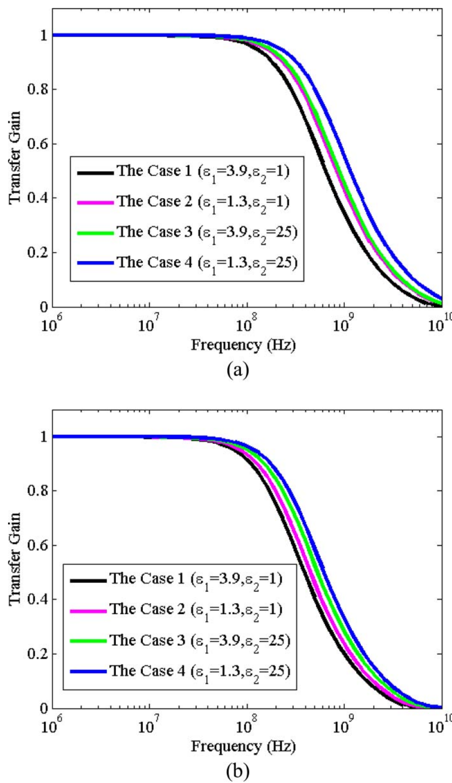

FIGURE 10. **The frequency response of center line of three-line coupled MLGNR interconnects with length L_{gnr} = 1000 μm for the defined four cases under in-phase crosstalk (a) and out-of-phase crosstalk (b) modes.**

greater propagation delay than two-line coupled MLGNR interconnects at the same case. For instance, in Fig. 7(b) and Fig. 9(b) for an interconnect length of $L_{gnr} = 4000$ μm, the propagation delay of case 1 for three-line coupled MLGNR interconnects is 54.783 ns while for two-line coupled MLGNR interconnects is 35.203 ns. Furthermore, the corresponding propagation delay of case 2, case 3 and case 4 for two-line coupled MLGNR interconnects are reduced by 42.34%, 35.46% and 40.51% respectively, as compared to three-line coupled MLGNR interconnects. The reason for this phenomenon is that the center line of three-line coupled MLGNR interconnects has greater coupling capacitance than the victim line of two-line coupled MLGNR interconnects in all same cases.

The frequency response of center line of three-line coupled MLGNR interconnects with length $L_{gnr} = 1000$ μm for the defined four cases under in-phase and out-of-phase crosstalk modes is described in Fig. 10(a) and 10(b), respectively. The frequency response results show that the three-line coupled MLGNR interconnects has the same behavior characteristic with the two-line coupled MLGNR interconnects. From the figures, in high frequency region, it is observed that the transfer gain for the case 2, case 3 and case 4 are obviously larger than that of the case 1 for in-phase and out-of-phase crosstalk modes. Meanwhile the proposed case 4 has greater transfer gain than the case 1, case 2 and case 3 for different phase crosstalk modes. Moreover, compared with Fig. 8(a) and 8(b) in high frequency region, it is found that the three-line coupled MLGNR interconnects have lower transfer gain than two-line coupled MLGNR interconnects at the same case. Taking the case 4 under in-phase mode at 1 GHz operating frequency as an example, the transfer gain for two-line coupled MLGNR interconnects is 0.781 while the value for three-line coupled MLGNR interconnects is 0.578. Based on the aforementioned discussion, the reason behind this is that the coupling capacitance exists only in the three-line coupled MLGNR interconnects for in-phase crosstalk mode according to the [40].

The 3-dB bandwidth of center line of three-line coupled MLGNR interconnects with different length for the defined four cases under in-phase and out-of-phase crosstalk modes are shown in Table 2. As can be observed from the Table, the three-line coupled MLGNR interconnects shows the same bandwidth performance pattern with the two-line coupled MLGNR interconnects. In addition, compared with Table 1, it is inferred that the 3-dB bandwidth of three-line coupled MLGNR interconnects is smaller than that of two-line coupled MLGNR interconnects at same conditions. Giving the interconnect length of $L_{gnr} = 3000$ μm under out-phase mode as an instance, the 3-dB bandwidth of two-line coupled MLGNR interconnects for case 1, case 2, case 3 and case 4 are 1.812, 1.708, 1.535 and 1.707 times larger than that of three-line coupled MLGNR

TABLE 2. **The bandwidth of center line of three-line coupled MLGNR interconnect with different length for the defined four cases under in-phase crosstalk and out-of-phase crosstalk modes.**

Length (μm)	3-dB bandwidth (MHz)							
	In-phase crosstalk mode				Out-of-phase crosstalk mode			
	Case 1	Case 2	Case 3	Case 4	Case 1	Case 2	Case 3	Case 4
100	1452.588	1533.634	1970.002	2087.538	1180.438	1308.053	1681.747	1771.136
200	640.633	705.968	874.171	968.352	457.597	538.243	677.647	735.870
400	250.934	294.430	342.998	405.371	154.050	193.049	236.304	265.395
600	136.266	166.718	186.267	229.829	76.980	99.608	120.071	137.230
800	85.967	108.302	117.491	149.398	46.107	60.812	72.619	83.878
1000	59.273	76.292	80.995	105.285	30.686	40.987	48.638	56.576
1500	29.314	39.057	41.043	53.931	14.395	19.583	23.025	27.060
2000	17.457	23.737	24.840	32.787	8.325	11.439	13.381	15.814
3000	8.235	11.456	12.243	15.829	3.806	5.285	6.149	7.310
4000	4.777	6.729	7.121	9.299	2.172	3.032	3.518	4.295

interconnects. This explanation is similar to the case of frequency response. As mentioned above, the two-line coupled MLGNR interconnects have smaller coupling capacitance than three-line coupled MLGNR interconnects at the same condition. Therefore, the former will have a larger cut-off frequency in comparison to the latter.

However, it should be pointed out that there are still some fundamental issues unresolved for the presented results. In this work, Joule heating and electrostatic reliability are not discussed, which will be the research subjects of our future work. Because the increase of Joule heating will give rise to interconnect temperature, thereby leading to the decrease of MFP λ_{eff} of MLGNR interconnect in VLSI circuits. Meanwhile electrostatic reliability is a paramount parameter to evaluate the performance of on-chip MLGNR interconnect due to the existing coupling capacitance and mutual inductance between adjacent lines.

V. CONCLUSION

An equivalent distributed circuit model of the proposed new technology for coupled MLGNR interconnects (i.e., the proposed case 4) is established to derive the mathematical expressions of step response, transfer gain and 3-dB bandwidth for 7.5 nm technology node at global level, which take the coupling capacitance and mutual inductance into account. By using the extracted interconnect parameters, the impacts of the defined four cases on step response, propagation delay, transfer gain and 3-dB bandwidth of the coupled interconnects are predicted. The numerical simulation results show that substituting the conventional MLGNR interconnects (i.e., the case 1) with the proposed case 4 for the coupled MLGNR interconnects has an obvious performance advantage in terms of the step response, propagation delay, transfer gain and 3-dB bandwidth at the same conditions. Besides, it is demonstrated that the coupled MLGNR interconnect under in-phase crosstalk mode has excellent advantage than that under out-of-phase mode with respect to lesser propagation delay, higher transfer gain and larger 3dB-bandwidth. Compared with two-line coupled MLGNR interconnects, the three-line coupled MLGNR interconnects have larger propagation delay, lower transfer gain and smaller 3-dB bandwidth at the same condition. In the light of our simulation results, it is manifested that the proposed new technology may be an emerging technology to improve the performance of step response, propagation delay, transfer gain and 3-dB bandwidth of the coupled MLGNR interconnects in VLSI circuits.

REFERENCES

[1] F. Liang, G. Wang, and H. Lin, "Modeling of crosstalk effects in multiwall carbon nanotube interconnects," *IEEE Trans. Electromagn. Compat.*, vol. 54, no. 1, pp. 133–139, Feb. 2012.

[2] A. Bagheri, M. Ranjbar, S. H. Nasiri, and S. Mirzakuchaki, "Crosstalk bandwidth and stability analysis in graphene nanoribbon interconnects," *Microelectron. Rel.*, vol. 55, no. 8, pp. 1262–1268, May 2015.

[3] W.-S. Zhao *et al.*, "Vertical graphene nanoribbon interconnects at the end of the roadmap," *IEEE Trans. Electron Devices*, vol. 65, no. 6, pp. 2632–2637, Jun. 2018.

[4] M. K. Rai, H. Garg, and B. K. Kaushik, "Temperature-dependent modeling and crosstalk analysis in mixed carbon nanotube bundle interconnects," *J. Electron. Mater.*, vol. 46, no. 8, pp. 5324–5337, Aug. 2017.

[5] A. Bagheril, M. Ranjbar, S. Haji-Nasiri, and S. Mirzakuchaki, "Modeling and analysis of crosstalk induced noise effects in bundle SWCNT interconnects and its impact on signal stability," *J. Comput. Electron.*, vol. 16, no. 3, pp. 845–855, Sep. 2017.

[6] P. Xu, Z. Pan, and Z. Tang, "The ultra-low-*k* dielectric materials for performance improvement in coupled multilayer graphene nanoribbon interconnects," *Electronics*, vol. 8, no. 8, pp. 1–12, Jul. 2019.

[7] I. N. Hajj, "On device modeling for circuit simulation with application to carbonnanotube and graphene nano-ribbon field effect transistor," *IEEE Trans. Comput.-Aided Design Integr. Circuits Syst.*, vol. 34, no. 3, pp. 495–499, Mar. 2015.

[8] L. B. Qian, Y. S. Xia, and G. Shi, "Study of crosstalk effect on the propagation characteristics of coupled MLGNR interconnects," *IEEE Trans. Nanotechnol.*, vol. 15, no. 5, pp. 810–819, Sep. 2016.

[9] L. Gengchiau, N. Neophytos, D. E. Nikonov, and M. S. Lundstrom, "Performance projections for ballistic graphene nano-ribbon field-effect transistor," *IEEE Trans. Electron Devices*, vol. 54, no. 4, pp. 667–682, Apr. 2007.

[10] L. Qian, Y. Xia, S. Ge, Y. Ye, and J. Wang, "Stability analysis for coupled multilayer graphene nanoribbon interconnects," *Microelectron. J.*, vol. 58, pp. 32–38, Dec. 2016.

[11] W.-S. Zhao and W.-Y. Yin, "Comparative study on multilayer graphene nanoribbon (MLGNR) interconnects," *IEEE Trans. Electromagn. Compat.*, vol. 56, no. 3, pp. 638–645, Jun. 2014.

[12] S. Kanthamani, G. Gayathiri, and S. Rohini, "Meshless analysis of bilayer graphene nanoribbon for radio frequency interconnects," *Micro. Nano. Lett.*, vol. 10, no. 11, pp. 613–616, Nov. 2015.

[13] V. R. Kumar, M. K. Majumder, and B. K. Kaushik, "Graphene based on-chip interconnects and TSVs: Prospects and challenges," *IEEE Nanotechnol. Mag.*, vol. 8, no. 4, pp. 14–20, Dec. 2014.

[14] P. Xu and Z. Pan, "Thermal model for three-dimensional integrated circuits with integrated MLGNR-based TSV," *Therm. Sci.*, to be published.

[15] V. Kumar, S. Rakheja, and A. Naeemi, "Performance and energy-per-bit modeling of multilayer graphene nanoribbon conductors," *IEEE Trans. Electron Devices*, vol. 59, no. 10, pp. 2753–2761, Oct. 2012.

[16] A. K. Nishad and R. Sharma, "Performance improvement in SC-MLGNRs interconnects using interlayer dielectric insertion," *IEEE Trans. Emerg. Topics Comput.*, vol. 3, no. 4, pp. 470–482, Dec. 2015.

[17] A. H. Neto, F. Guinea, N. M. R. Peres, K. S. Novoselov, and A. K. Geim, "The electronic properties of graphene," *Rev. Mod. Phys.*, vol. 81, no. 1, pp. 1–56, Jan. 2009.

[18] K. Hosono and K. Wakabayashi, "Dielectric environment effect on carrier mobility of graphene double-layer structure," *Appl. Phys. Lett.*, vol. 103, Jul. 2013, Art. no. 033102.

[19] G. K. Mekala, Y. Agrawal, and R. Chandel, "Modeling and performance analysis of dielectric inserted side contact multilayer graphene nanoribbon interconnects," *IET Circuit Device. Syst.*, vol. 11, no. 3, pp. 232–240, Jun. 2017.

[20] C. R. Dean *et al.*, "Boron nitride substrates for high quality graphene electronics," *Nat. Nanotechnol.*, vol. 5, no. 10, pp. 722–726, Oct. 2010.

[21] L. Liao, J. Bai, Y. Qu, Y. Huang, and X. Duan, "Single-layer graphene on Al_2O_3/Si substrate: Better contrast and higher performance of graphene transistors," *Nanotechnology*, vol. 21, no. 1, pp. 1–5, Jan. 2010.

[22] K. Zou, X. Hong, D. Keefer, and J. Zhu, "Deposition of high-quality HfO_2 on graphene and the effect of remote oxide phonon scattering," *Phys. Rev. Lett.*, vol. 105, no. 12, Sep. 2010, Art. no. 126601.

[23] M. Kaur, N. Gupta, and A. K. Singh, "Crosstalk analysis of coupled MLGNR interconnects with different types of repeater insertion," *Microprocess. Microsyst.*, vol. 67, pp. 18–27, Jun. 2019.

[24] S. Bhattacharya, D. Das, and H. Rahaman, "Analysis of delay fault in GNR power interconnects," *Int. J. Numer. Model.*, vol. 31, no. 8, pp. 1–16, May/Jun. 2018.

[25] M. K. Rai, A. K. Chatterjee, S. Sarkar, and B. K. Kaushik, "Performance analysis of multilayer graphene nanoribbon (MLGNR) interconnects," *J. Comput. Electron.*, vol. 15, no. 2, pp. 358–366, Jan. 2016.

[26] M. K. Rai, S. Arora, and B. K. Kaushik, "Temperature-dependent modeling and performance analysis of coupled MLGNR interconnects," *Int. J. Circuit Theor. Appl.*, vol. 46, no. 3, pp. 299–312, Jul. 2017.

[27] S. Das, D. Das, and H. Rahaman, "Electro-thermal RF modeling and performance analysis of graphene nanoribbon interconnects," *J. Comput. Electron.*, vol. 17, no. 4, pp. 1695–1708, Dec. 2018.

[28] J.-P. Cui, W.-S. Zhao, W.-Y. Yin, and J. Hu, "Signal transmission analysis of multilayer graphene nano-ribbon (MLGNR) interconnects," *IEEE Trans. Electromagn. Compat.*, vol. 54, no. 1, pp. 126–132, Feb. 2012.

[29] M. K. Majumder, N. R. Kukkam, and B. K. Kaushik, "Frequency response and bandwidth analysis of multi-layer graphene nanoribbon and multi-walled carbon nanotube interconnects," *Micro. Nano. Lett.*, vol. 9, no. 9, pp. 557–560, Sep. 2014.

[30] A. Alam, M. K. Majumder, A. Kumari, V. R. Kumar, and B. K. Kaushik, "Performance analysis of single-and multi-walled carbon nanotube based through silicon vias," in *Proc. IEEE 65th Electron. Compon. Technol. Conf.*, San Diego, CA, USA, 2015, pp. 1834–1839.

[31] R. Kar, V. Maheshwari, M. Maqbool, S. Mondal, A. K. Mal, and A. K. Bhattacharjee, "Crosstalk aware bandwidth modeling for distributed on-chip RLCG interconnects using difference model approach," in *Proc. IEEE Int. Conf. Comput. Commun. Netw. Technol.*, 2010, pp. 1–5.

[32] T. Kaur, M. K. Rai, and R. Khanna, "Effect of temperature on the performance analysis of MLGNR interconnects," *J. Comput. Electron.*, vol. 18, no. 2, pp. 722–736, Jun. 2019.

[33] Y. Agrawal, M. G. Kumar, and R. Chandel, "A novel unified model for copper and MLGNR interconnects using voltage-and current-mode signaling schemes," *IEEE Trans. Electromagn. Compat.*, vol. 59, no. 1, pp. 217–227, Feb. 2017.

[34] S. H. Nasiri, "Compact Formulae for number of conduction channels in various types of graphene nanoribbons at various temperatures," *Mod. Phys. Lett. B*, vol. 26, no. 1, Jan. 2012, Art. no. 1150004.

[35] M. Sahoo and H. Rahaman, "Modeling and analysis of crosstalk induced overshoot/undershoot effects in multilayer graphene nanoribbon interconnects and its impact on gate oxide reliability," *Microelectron. Rel.*, vol. 63, pp. 1–8, Jun. 2016.

[36] F. Stellari and A. L. Lacaita, "New formulas of interconnect capacitances based on results of conformal mapping method," *IEEE Trans. Electron Devices*, vol. 47, no. 1, pp. 222–231, Feb. 2000.

[37] *ITRS International Technology Working Groups*, Int. Technol. Roadmap Semicond., London, U.K., 2011.

[38] P. Xu and Z. Pan, "The analytical model for crosstalk noise of current-mode signaling in coupled RLC interconnects of VLSI circuits," *J. Semicond.*, vol. 38, no. 9, pp. 1–8, Sep. 2017.

[39] V. R. Kumar, M. K. Majumder, N. R. Kukkam, and B. K. Kaushik, "Time and frequency domain analysis of MLGNR interconnects," *IEEE Trans. Nanotechnol.*, vol. 14, no. 3, pp. 484–492, May 2015.

[40] T. Kim and Y. Eo, "Analytical CAD models for the signal transients and crosstalk noise of inductance-effect-prominent multicoupled RLC interconnect lines," *IEEE Trans. Comput.-Aided Design Integr. Circuits Syst.*, vol. 27, no. 7, pp. 1214–1227, Jul. 2008.

[41] S. Adam, E. H. Hwang, V. M. Galitski, and S. D. Sarma, "A self-consistent theory for graphene transport," *Proc. Nat. Acad. Sci. USA*, vol. 104, no. 47, pp. 18392–18397, 2007.

[42] P. Xu and Z. Pan, "The insertion of high-*k* dielectric materials in multilayer graphene nanoribbon interconnects for reducing propagation delay and expanding bandwidth," *Org. Electron.*, vol. 78, pp. 1–7, Mar. 2020.

PENG XU received the B.Eng. degree in electronic information science and technology from Xiangnan University, Chenzhou, China, in 2013, and the M.Eng. degree in circuits and systems from South China Normal University, Guangzhou, China, in 2017, where he is currently pursuing the Ph.D. degree in microelectronics and solid state electronics. His current research interests are focused on modeling and performance enhancing of high-speed MLGNR-based interconnects in very large scale integration circuits.

ZHONGLIANG PAN received the Ph.D. degree in circuits and systems from the University of Electronic Science and Technology of China, Chendu, China, in 1997. He was a Postdoctoral Research Associate with Sun Yat-sen University, Guangzhou, China, from 1998 to 1999. Since 2004, he has been a Professor with the School of Physics and Telecommunication Engineering, South China Normal University, Guangzhou. His current research interests include the system-level design and testing of very large scale integration circuits.